

# The influence of geometry on inviscid decay rates in haemodynamic flows

By M. G. BLYTH AND A. J. MESTEL

Mathematics Department, Imperial College, 180 Queen's Gate, London SW7 2BZ, UK

(Received 18 December 2000 and in revised form 27 September 2001)

Fully developed flows are often used to describe fluid motion in complex geometrical systems, including the human macrocirculation. In fact they may frequently be quite inappropriate even for geometrically simple pipes, owing to the unfeasibly large viscous entry lengths required. Inviscid adjustment to changes in geometry, however, occurs on the lengthscale of the pipe diameter. Inviscid idealizations are therefore more likely to apply in relatively short arterial sections. We aim to quantify the distances involved by calculating the rates of spatial decay for a general disturbance superimposed on an idealized base flow. Both irrotational and rotational base flows are examined, although in the latter case there can exist non-decaying inertial waves, so that an arbitrary inflow need not attain an inviscid state independent of the downstream coordinate. In the rotational case, we therefore restrict attention to those flows which settle down to perturbations of such a state, whereas the potential flows can be regarded as developing from an arbitrary input.

We focus on the last surviving mode of decay in simple uniform pipe geometries, in particular a straight pipe, part of a torus, and a helical pipe. In this way we are able to assess the effects of curvature and torsion on the inviscid entry lengths.

Principally, it is shown that the rate of decay is fastest in a straight pipe and slowest in a toroidal pipe, with that in a helical pipe somewhere in between. Core vorticity tends to reduce the decay rate. If an idealized flow occurs in a geometrically simple arterial portion, our results determine its domain of validity.

---

## 1. Introduction

There is a wide variety of theoretical pipe flow applications in engineering (see, for example, the review article by Berger, Talbot & Yao 1983). Such analytical studies can also be helpful in the understanding of physiological flows (Ku 1997). In either case, the competition of many different factors increases the difficulty of producing a tractable mathematical model. In the human body, for example, flow prediction in the larger blood vessels is complicated by their elaborate geometry. This is frequently non-planar, and involves a large number of bends and bifurcations. The geometry may even vary with time, as for the extra-myocardial coronary arteries (Lynch, Waters & Pedley 1996). In addition, the driving pressure gradient, though essentially periodic, has a non-trivial time-dependence.

Fully developed idealized models are commonly used to describe the flow in such situations. For example, steady Dean (1927, 1928) flow has been used to model fluid motion at some distance from the heart, while flow in helical pipes (Zabielki & Mestel 1998*a, b*) has been studied with reference to the aortic arch. In practice, real flows may have insufficient space to adjust to the asymptotic state. While some flows require an

entry length of order the Reynolds number, the rapidly oscillating Womersley-like flows require a much shorter distance. Adjustment of inviscid cores likewise occurs over a length of order the pipe diameter. In this paper we address the question of how rapidly these states are reached. For example, if a curved pipe straightens out, it would be of practical interest to know over what lengthscale the residual swirl from the final bend dies out. This question is of fundamental importance to the suitability of using simplified models to describe real flows. Accurate measures of entry and exit lengths also improve the efficiency of computational studies.

We investigate both rotational and irrotational inviscid flows. Initially we argue that, given appropriate entry and exit conditions, rapidly oscillating Womersley-type flows in pipes of quite complex geometry may be considered to be potential, with viscous effects confined to thin Stokes layers at the walls. The entry problem for potential flows can be formulated for an arbitrary input, but we concentrate on the final decay before the flow settles to its inviscid downstream limit. Subsequently we discuss the evolution of inviscid flows with a rotational core, again assuming that at sufficiently high Reynolds numbers viscous effects are unimportant away from the walls. Such flows might be applicable further along the arterial tree where the fluctuating component of the pressure has weakened. With vorticity present there is the possibility of inertial waves which do not decay with downstream distance. Such waves have been found by, for example, Sobey (1976) in a pipe of slowly varying elliptical cross-section, and Pedley & Stephanoff (1985) in a channel with a time-dependent indentation. Thus, although a contained Euler flow with a general rotational input need not evolve to a downstream-invariant state, we focus our attention on those flows which are observed to do so, and analyse the rates at which this equilibration takes place. From a haemodynamic standpoint, we argue that should a cross-sectional scan indicate a flow almost consistent with downpipe invariance, then our results can be used to estimate the domain of validity of an idealized model. In this spirit we examine inviscid flows in three characteristic types of geometry: a straight pipe; a section of a torus; and a helical pipe. These allow us to quantify the effects of curvature and torsion on the decay rate.

For potential flow, separable eigenfunctions with exponential downpipe behaviour may be found for the straight pipe and torus section. Analysis for the helical pipe is hampered by the lack of an orthogonal coordinate system, and progress is made by numerical means. In all cases we consider pipes with a rectangular or circular cross-section, the latter having the greater physiological relevance.

Rotational flows are discussed in the latter half of the paper. Decaying disturbances to the steady-state unidirectional flow in a straight pipe are examined, both with and without wall slip. In the latter, corresponding to the fully developed viscous state, unsteady modes are found to be important. Inviscid decay in curved sections is also studied. To this end, flow at high Dean number is adopted as the base state, and the evolution of small perturbations analysed. Some previous authors have studied the steady high-Dean-number entry problem analytically (Singh 1974; Yao & Berger 1975; Stewartson, Cebeci & Chang 1980) and experimentally (Agrawal, Talbot & Gong 1978). In our work small curvature is assumed for pipes with circular cross-sections, while pipes of arbitrary, but uniform, curvature with rectangular cross-sections are also considered. For the former case at least, the background flow is itself non-trivial and the full asymptotic problem, incorporating the viscous boundary layer at the wall, is still not satisfactorily resolved. However, numerical calculations, for example by Collins & Dennis (1975), and theoretical work, by Smith (1976*a*) for triangular and rectangular cross-sections, and more recently by Dennis & Riley

(1991), have provided mounting evidence that the dual, counter-rotating vortex pair representation, with the boundary layer everywhere attached and no eruption into the core, is valid at large finite Dean number and therefore we adopt this as our base flow.

Some of this work is related to spatial stability problems. Here, we assume implicitly that the underlying flows are stable, and seek the perturbation which decays slowest. A general discussion of spatially developing flows is given by Huerre & Monkewitz (1990).

## 2. Preliminaries

### 2.1. Decay rates

Flow in a tube with downpipe symmetry, for example a torus, can reasonably be expected to achieve a corresponding symmetry given a sufficient entry length. The distance required for viscous effects to act is long, but in some circumstances an inviscid symmetric state can be achieved rapidly, which is the subject of the current study. Potential flows are considered in §3, while vorticity effects are introduced in §4.

The potential problem is formulated as follows. Given a unit symmetry direction, denoted  $\hat{s}$ , we choose our coordinate system, denoted  $(x_1, x_2, x_3)$ , so that  $\hat{s}$  is perpendicular to the  $(x_1, x_2)$ -plane. This coordinate system is not necessarily orthogonal. A pipe, denoted  $\Omega$ , is generated by continuously translating a closed boundary curve  $\partial\Omega_c : F(x_1, x_2) = 0$ , and its interior  $\Omega_c$ , in the direction of  $\hat{s}$ . Solutions of Laplace's equation,  $\nabla^2 V = 0$ , are then sought in  $\Omega$  subject to tangential flow boundary conditions,  $\mathbf{n} \cdot \nabla V = 0$ , on  $\partial\Omega_c$ . The vector  $\mathbf{n}$  is normal to the boundary. The solutions are assumed to take the generic form

$$V = V_0(x_1, x_2, x_3) + \sum_{n=1}^{\infty} V_n(x_1, x_2) e^{-k_n x_3}, \quad (2.1)$$

for constant eigenvalues  $\text{Re}\{k_n\} > 0$ , and some appropriately chosen third coordinate  $x_3$ . In the downstream limit,  $x_3 \rightarrow \infty$ , the flow  $\mathbf{u}_0 = \nabla V_0$  satisfies  $\hat{s} \cdot \nabla \mathbf{u}_0 = \mathbf{0}$ , and so the potential  $V_0$  is at most linear in  $x_3$ . Determining the smallest  $k_n$  establishes the slowest decay rate at which this developed flow  $\mathbf{u}_0$  is approached. Decay rates in rotational flows are treated in a similar manner, the Euler equations being linearized about the developed state. In that case, some of the modes can be neutral, with  $\text{Re}\{k_n\} = 0$ .

Since we are mostly dealing with homogeneous Neumann problems, we will throughout ignore the zeroth trivial eigenvalue and associated eigenfunction and use 'first' to mean the first non-zero eigenvalue. In the same way, we will use the term 'smallest' in connection with eigenvalues to mean one with the smallest strictly positive real part. Also, we will refer to a toroidal or helical pipe with a circular or rectangular cross-section as a circular or rectangular torus or helix respectively. We will frequently make reference to the axes  $(x, y, z)$  of the Cartesian frame, and cylindrical polars  $(r, \theta, z)$ , with respective unit vectors  $(\mathbf{e}_r, \mathbf{e}_\theta, \mathbf{e}_z)$ . The cylindrical coordinates are shown with three typical pipe geometries in figure 1.

### 2.2. Motivation for studying potential flow

Consider the motion of a fluid of density  $\rho$  and kinematic viscosity  $\nu$  inside a three-dimensional pipe of typical width  $a$ , driven by a pressure gradient oscillating at frequency  $\omega$ . Let the fluid velocity at the inlet have typical magnitude  $U$  and the

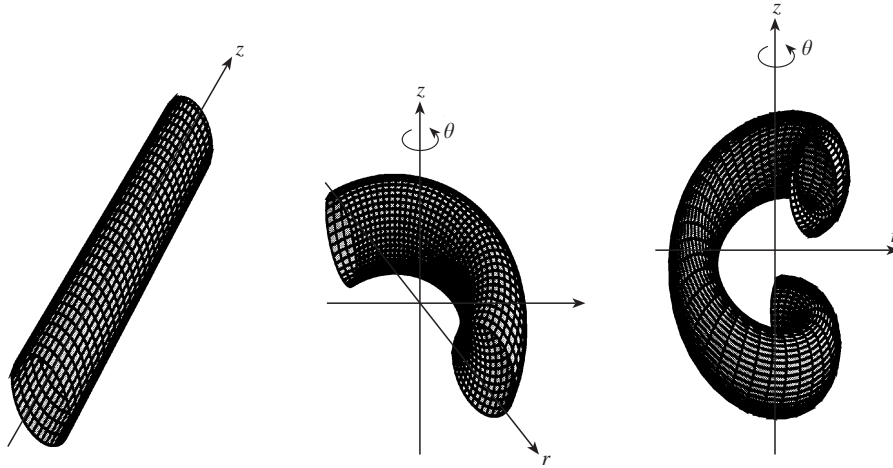


FIGURE 1. The three pipe geometries in cylindrical coordinates  $(r, \theta, z)$ : a straight pipe, a section of a torus of uniform curvature, and a helical pipe of constant curvature and pitch. Rectangular cross-sections are also considered.

entrance flow be irrotational. If we divide velocities by  $U$ , the pressure by  $\rho U^2$ , and time by  $1/\omega$ , we may write the unsteady Navier–Stokes equations as

$$\alpha^{-2} \mathbf{u}_t + \mathbf{u} \cdot \nabla \mathbf{u} = -\nabla p + R^{-1} \nabla^2 \mathbf{u}, \quad \nabla \cdot \mathbf{u} = 0, \quad (2.2)$$

where  $\alpha^2$  is defined to be  $U/(\omega a) = Rv/(\omega a^2)$ , and  $R = Ua/v$  is the Reynolds number for the flow. When  $\alpha \ll \min\{1, R^{1/2}\}$ , a simple structure occurs with an irrotational core and Stokes layers.

In the mammalian macrocirculation, the driving pressure gradient has a relatively small steady component, while the fluctuating and mean velocities are comparable (McDonald 1974). In (2.2), writing  $\nabla p = \nabla p_0(\mathbf{x}, t) + \nabla p_1(\mathbf{x})$ , where  $|\nabla p_0| \gg |\nabla p_1|$ , and  $\mathbf{u} = \mathbf{u}_0(\mathbf{x}, t) + \mathbf{u}_1(\mathbf{x})$ , yields at leading order  $\mathbf{u}_{0t} = -\nabla p_0$ . The unsteady part of the core flow is therefore potential. Furthermore, this flow is established over a distance of  $O(U/\omega) \ll aR$  (Pedley 1980). The fully developed steady core flow is not irrotational, as viscous effects, including steady streaming from the Stokes layers, eventually become important. However, if the entry flow is irrotational, then it will remain so on a downpipe lengthscale small compared to  $R$ . Denoting a time-average by an overline, the steady potential flow requires that

$$p_1 + \frac{1}{2} \mathbf{u}_1^2 + \frac{1}{2} \overline{\mathbf{u}_0^2} = \text{const.}$$

Upon averaging this relation over a pipe cross-section, it can be seen that a drop in mean pressure can result not only because of viscous resistance, but also from growing complexity of the pipe geometry. When a straight artery bends, the potential velocity becomes non-uniform, so that its mean-square increases and thus the mean pressure decreases.

Potential flows are thus crucial in the high-frequency Womersley limit  $\alpha \ll 1$ , certainly for the oscillatory flow, and possibly even for the steady component. However, this limit is not attained in the larger human arteries such as the aorta, as the non-linear term is important. Nevertheless, for general  $\alpha$  an initially irrotational core flow remains irrotational until a wall layer separates or diffuses. For non-straight pipes centrifugal effects in the boundary layers generate secondary cross-pipe flows. For

a uniform bend, in a pipe of radius  $a$  and radius of curvature  $b$  say, these layers separate at the inner wall a distance  $3.98a(b/(2a))^{1/2}$  downstream of the inlet (Riley 1998; see also Lam 1988). In the human aortic arch the ratio  $a/b$  is approximately 0.4 (Chandran 1993), suggesting that the flow is potential for the first  $102^\circ$  of the bend. Analyses of other viscous entry flow problems are given by Pedley (1980). Here we concentrate on the leading-order potential flow and in particular investigate its form for differing pipe geometries.

### 3. Decay rates in potential flow

#### 3.1. Straight pipes

##### 3.1.1. Rectangular

For a straight pipe aligned with the  $z$ -axis, we seek solutions which are exponentially decaying in  $z$ . Therefore in §2.1 we have  $\hat{s} = e_z$  and  $x_3 = z$ . For a rectangular pipe with cross-section  $x = 0, \pi a_0$  and  $y = 0, \pi b_0$ , we find

$$V_n = \cos(lx/a_0) \cos(my/b_0) \exp(-k_n z), \quad \text{where } k_n^2 = l^2/a_0^2 + m^2/b_0^2,$$

for integer  $l, m$ . The first eigenvalue is therefore given by  $k_1 = 1/\max\{a_0, b_0\}$ . If  $a_0$  is equal to  $b_0$  this first eigenvalue is degenerate, since we could take  $(l, m)$  to be either  $(1, 0)$  or  $(0, 1)$ . From now on, we shall suppress the suffices on  $V_n$  and  $k_n$ , referring always to the first eigenmode.

##### 3.1.2. Circular

For a circular pipe at  $r = 1$ , the first eigenvalue is also degenerate, with eigenfunction either  $V = J_1(kr) \cos \theta$  or  $V = J_1(kr) \sin \theta$ , where  $J_1$  is the Bessel function of the first kind. The eigenvalues  $k$  satisfy  $J_1'(k) = 0$ , of which the smallest is  $k \simeq 1.841$ .

For both circular and rectangular shapes the last eigenfunction to decay has a '+/-' structure, with some dividing line on which the downpipe velocity vanishes.

#### 3.2. Toroidal pipes

##### 3.2.1. Rectangular

For a toroidal pipe of rectangular cross-section, it is natural to use cylindrical polar coordinates. Let  $r = b \pm a$ ,  $z = 0, z_0$  define the pipe's cross-section. We are concerned with a section of the torus over which perturbations decay exponentially in  $\theta$ . Hence periodicity in  $\theta$  is not imposed. So, with reference to §2.1, we now take  $\hat{s} = e_\theta$  and  $x_3 = \theta$ . For positive integer  $n$  the eigenfunction for this rectangular torus is

$$V = \exp(-\kappa\theta) \cos(n\gamma z) \operatorname{Re}\{J_{ic}(in\gamma r) + C J_{-ic}(in\gamma r)\}, \quad (3.1)$$

where  $\gamma = \pi/z_0$ , and  $C$  is an unknown real constant. The Neumann boundary conditions at  $r = b \pm a$  determine  $\kappa$  and  $C$  for a given  $n > 0$ . When  $n = 0$  we find

$$\frac{\pi}{\kappa} = \log \left( \frac{b+a}{b-a} \right). \quad (3.2)$$

In this case the eigenvalue is not degenerate. Depending on the pipe aspect ratio the smallest eigenvalue is determined either by (3.1) or (3.2). The eigenfunction has a similar +/− structure to those in §3.1.

##### 3.2.2. Circular

The calculation for the circle is more involved. In order to describe this flow it is most convenient to utilize toroidal coordinates  $(\mu, \eta, \theta)$  (see, for example, Morse &

Feschbach 1953). These are defined by rotating bipolar coordinates about the  $z$ -axis. Thus

$$z = a \sin \eta / h_\tau, \quad x = a \sinh \mu \cos \theta / h_\tau, \quad y = a \sinh \mu \sin \theta / h_\tau,$$

where  $h_\tau = \cosh \mu - \cos \eta$ . As above  $0 \leq \theta < 2\pi$  measures the angle around the  $z$ -axis. In a fixed  $\theta$ -plane, with  $\mu = \mu_0$  held constant,  $0 \leq \eta < 2\pi$  parameterize a family of circles of radius  $a / \sinh \mu_0$  and centre  $(x^2 + y^2)^{1/2} = a \coth \mu_0$ . The range  $\mu_0 \leq \mu < \infty$  corresponds to the interior of the torus with  $\mu = \mu_0$  as its boundary.

We seek solutions decaying azimuthally with  $\theta$ . In these coordinates the Laplacian is separable. Writing  $V = h_\tau^{1/2} F(\mu, \tau, \theta)$ , it becomes

$$\frac{1}{\sinh \mu} \frac{\partial}{\partial \mu} \left( \sinh \mu \frac{\partial F}{\partial \mu} \right) + \frac{\partial^2 F}{\partial \eta^2} + \frac{1}{\sinh^2 \mu} \frac{\partial^2 F}{\partial \theta^2} + \frac{1}{4} F = 0.$$

The solution may be written as

$$V = h_\tau^{1/2} \exp(-\kappa \theta) \sum_{m=0}^{\infty} \alpha_m \cos(m\eta) Q_{m-1/2}^{i\kappa}(\cosh \mu), \quad (3.3)$$

where the  $\alpha_m$  are constants and  $Q_{m-1/2}^{i\kappa}$  is the associated Legendre function of the second kind. A Dirichlet boundary condition would pose a straightforward problem for  $\kappa$ . However, since the square-root  $h_\tau$  factor is a function of  $\mu$ , the requirement that  $V_\mu = 0$  produces a mixed boundary condition on the toroidal surface. In fact, writing  $\xi = \cosh \mu$ , we ultimately require that

$$\alpha_m Q_{m-1/2}^{i\kappa} - \frac{d}{d\xi} (2\alpha_m \xi Q_{m-1/2}^{i\kappa} + \alpha_{m-1} Q_{m-3/2}^{i\kappa} - \alpha_{m+1} Q_{m+1/2}^{i\kappa}) = 0 \quad (3.4)$$

on  $\xi = \xi_0$  for all  $m$ . Accordingly all modes  $m$  contribute to a single eigenvalue  $\kappa$ . It is important to note at this stage that exactly the same condition as (3.4) is produced if we replace  $\cos(m\eta)$  in (3.3) with  $\sin(m\eta)$ . So the eigenvalue  $\kappa$  is degenerate for a circular torus of arbitrary curvature, unlike for the rectangular torus. There is no obvious geometrical symmetry to explain this, but it is related to the manner in which the Laplacian separates.

Truncating (3.3) at a value  $m = M$ , the condition (3.4) may be written as a matrix equation  $\mathbf{A}(\kappa)\boldsymbol{\alpha} = 0$ , where  $\boldsymbol{\alpha}$  is a column vector with  $m$ th entry  $\alpha_m$ . The determinant of  $\mathbf{A}$  has zeros which approach the eigenvalues  $\kappa$  as  $M \rightarrow \infty$ . To determine precisely where the matrix is singular we looked at the singular value decomposition of the matrix. The existence of an eigenvalue was decided at a point  $\kappa$  where the ratio of the smallest to the largest of the singular values was numerically zero. We took the cross-sectional radius  $a / \sinh \mu_0 = 1$ , and so the radius of curvature  $b = \cosh \mu_0$ . The results are shown in figure 2. As the radius of curvature  $b$  increases the curve asymptotes to 1.84, since this is the smallest eigenvalue for the straight pipe with unit radius (see above). In fact we find that  $\kappa/b \sim 1.84 - 0.72/b^2$  as  $b$  tends to infinity.

Finally we note that the eigenfunctions have a similar  $+/-$  structure to those in §3.1.

### 3.3. Helical pipes

In order to assess the effect of torsion on decay rate, we examine potential flow in a helical pipe. Such a geometry has recently been considered by Zabielski & Mestel (1998*a, b*) for both steady and unsteady flows. The former paper will henceforth be referred to as ZM. In both cases these authors were interested in flows which did

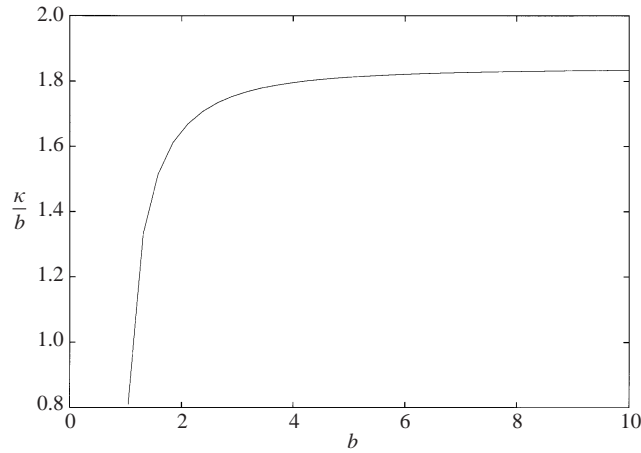


FIGURE 2. Variation of  $\kappa/b$  with radius of curvature  $b = \cosh(\mu_0)$  for a circular torus of radius  $a/\sinh \mu_0 = 1$ . As  $b \rightarrow \infty$ ,  $\kappa/b \rightarrow 1.84$  as expected.

not vary along the pipe in the direction of helical symmetry  $\mathbf{H}$ , defined below. The approach to such a helically symmetric potential solution is the subject of the current section.

Most of the details of the coordinate system and orthogonal helical vector base are given in ZM. In the interest of clarity, we will repeat some of these here. A left-handed helix is parameterized in a Cartesian  $(x, y, z)$  frame as  $(x, y, z) = (r \cos(\varepsilon t), -r \sin(\varepsilon t), t)$  for constant pitch  $\varepsilon > 0$ . In terms of cylindrical coordinates  $(r, \theta, z)$ , a base of orthogonal unit vectors is defined by

$$\mathbf{e}_r = \mathbf{e}_r, \quad \mathbf{e}_\phi = h\mathbf{H} \times \mathbf{e}_r = (\mathbf{e}_\theta + \varepsilon r \mathbf{e}_z)/h, \quad \mathbf{e}_H = h\mathbf{H} = (-\varepsilon r \mathbf{e}_\theta + \mathbf{e}_z)/h, \quad (3.5)$$

where  $h(r) = (1 + \varepsilon^2 r^2)^{1/2}$ . Then the helix of radius  $r = b$  has curvature  $\varepsilon^2 b/h_b^2$ , where  $h_b = h(b)$ , and torsion  $-\varepsilon/h_b^2$ . A scalar function  $f$  is defined to be helically symmetric when  $\mathbf{H} \cdot \nabla f = 0$ . The two limits  $\lim_{\varepsilon \rightarrow 0} \mathbf{e}_H = \mathbf{e}_z$  and  $\lim_{\varepsilon \rightarrow \infty} \mathbf{e}_H = -\mathbf{e}_\theta$  correspond to two-dimensionality (straight pipe) and axisymmetry (torus) respectively.

The fact that  $\nabla \times (h\mathbf{e}_\phi/r) = 0$  enables us to define a new coordinate  $\phi = \theta + \varepsilon z$ . However, it is impossible to define a third orthogonal coordinate (see ZM). This is not important when dealing with helical symmetry, but it is somewhat inconvenient if, as here, we wish to allow variation in the  $\mathbf{H}$ -direction.

### 3.3.1. Rectangular helix

It is most straightforward to begin by considering the rectangular curve  $r = b \pm a$ ,  $\phi = 0, \phi_0$ . When translated continuously in the  $\mathbf{H}$ -direction, this defines a helical pipe. For non-zero torsion it can be viewed as having a rectangular cross-section in physical space (at  $\theta = 0$  for example). When  $\varepsilon = 0$  it defines a straight pipe whose cross-section is a truncated wedge. At  $\varepsilon = \infty$  it is a rectangular torus.

We seek solutions which decay exponentially along the pipe. The lack of a third orthogonal coordinate obscures what we mean by ‘along’ here, so although we set  $\hat{s} = h\mathbf{H}$  in §2.1, it is not yet clear what to take for  $x_3$ . We wish to solve Laplace’s equation for  $V$ , such that  $h\mathbf{H} \cdot \nabla V = \beta(r, \phi)V$ , for some function  $\beta$ . To satisfy this requirement, we may choose  $\beta = k/h$  (so  $x_3 = z$  or  $x_3 = -\theta/\varepsilon$ ), and write

$$V = e^{-kz} f(r, \phi) = e^{\kappa\theta} g(r, \phi), \quad (3.6)$$

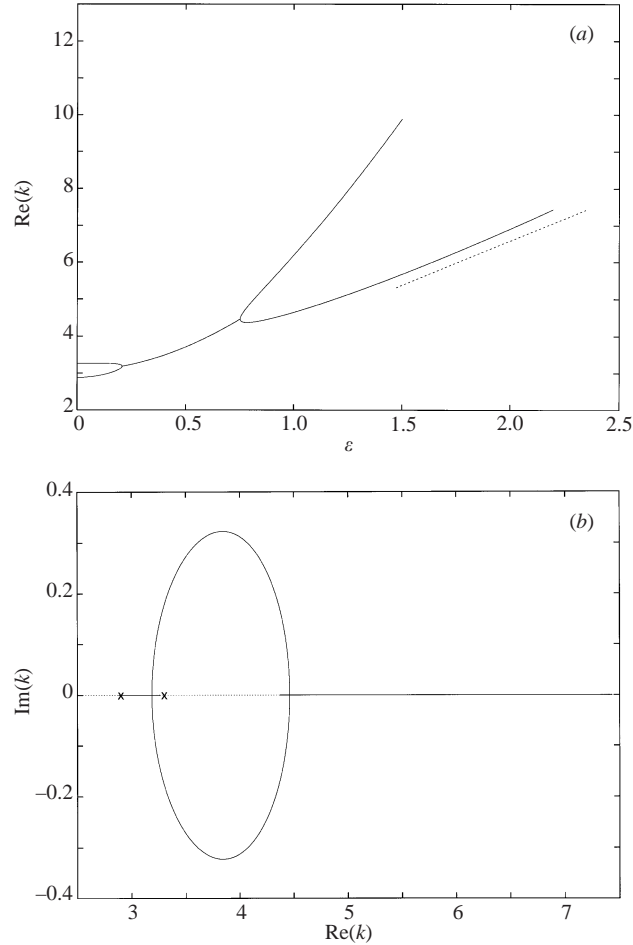


FIGURE 3. Numerical solution for a pipe with  $\phi = 1.0$ ,  $r = 1 \pm 0.5$ . Plots are shown for the first and second eigenvalues. (a)  $\text{Re}(k)$  against  $\varepsilon$ , (b)  $\text{Re}(k)$  and  $\text{Im}(k)$  varying with  $\varepsilon$ . The points  $\times$  indicate where  $\varepsilon = 0$ . The straight dotted line in (a) has gradient 2.86 (see text). The two bifurcation points in (a) correspond to where the solution changes from real to complex, and complex to real respectively in (b).

where  $k$ ,  $\kappa (= k/\varepsilon)$  are both constants. The helically symmetric functions  $f$  and  $g$  are related by  $g = \exp\{-\kappa\phi\}f$ . In these coordinates, Laplace's equation becomes

$$f_{rr} + f_r/r + h^2 f_{\phi\phi}/r^2 - 2\varepsilon k f_\phi + k^2 f = 0, \quad (3.7)$$

with boundary conditions  $f_r = 0$  at  $r = b \pm a$ , and  $h^2 f_\phi/r^2 - \varepsilon k f = 0$  at  $\phi = 0, \phi_0$ . As this problem is not self-adjoint  $k$  and  $f$  may be complex, in which case the real part is implicit in (3.6). It is solved numerically using centred differences for the derivatives. The resulting system is written in the matrix form  $\mathbf{A}\mathbf{f} = \mathbf{0}$ , where  $\mathbf{f}$  is the vector of  $f$  values at each grid point, and  $\mathbf{A}$  has entries which are at most quadratic in  $k$ . Newton iteration is used based on the method of Lancaster (1966, p. 78). A  $(15 \times 15)$  grid is sufficient to compute the eigenvalues with a relative accuracy of  $10^{-3}$ . The eigenvalues were tracked as  $\varepsilon$  increases from 0. In figure 3 we can see the behaviour of the complex first and second eigenvalues with varying  $\varepsilon$ .

At  $\varepsilon = 0$  we have a straight pipe, whose cross-section is the truncated wedge



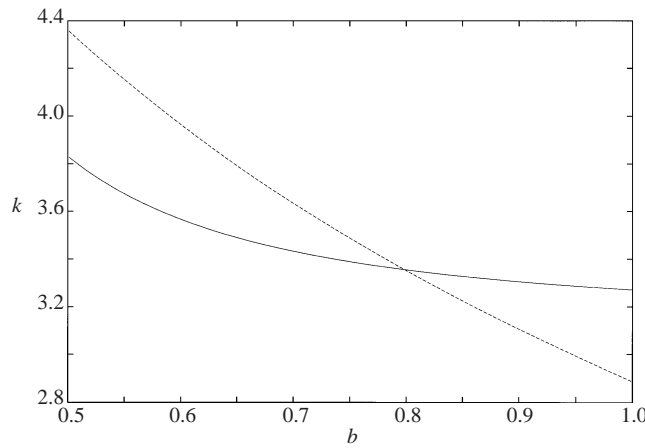


FIGURE 4. Merging of two roots for straight truncated wedge pipe.  $a = 0.5$ . The solid line is  $n = 0$ , dashed is  $n = 1$ . Note as  $b \rightarrow \infty$ , the solid line tends to  $\pi$  and the dashed line decreases monotonically.

$r \in [0.5, 1.5]$ ,  $\theta \in [0, 1]$ . We find the first eigenvalue  $k = 2.886$ , and the second  $k = 3.271$ . Thereafter as  $\varepsilon$  is increased these two eigenvalues eventually coalesce to form a complex-conjugate pair in the approximate range  $0.208 < \varepsilon < 0.753$ , whereafter they rejoin and subsequently diverge as separate real values.

It is informative to monitor the effect of varying  $b$  on the first bifurcation point in figure 3(a). We find that when it is decreased from its current value  $b = 1$ , the bifurcation point moves closer to the  $\text{Re}(k)$ -axis, eventually touching it before bouncing back. This suggests a degeneracy in the first eigenvalue for the straight truncated wedge pipe. Such a pipe has eigenfunction

$$V = \exp(-kz) \cos(n\pi\theta) \{J_n(kr) + C J_{-n}(kr)\}, \tag{3.8}$$

for integer  $n$ , and constant  $C$ . Fixing the width  $2a = 1$ , we find that for most of the range  $0 \leq b < \infty$ , the smallest eigenvalue for this straight pipe corresponds to  $n = 1$ . However, as can be seen in figure 4, for a small range of  $b$ ,  $n = 0$  contributes the smallest  $k$ , with degeneracy of the eigenvalue occurring at  $b \simeq 0.8$ .

The iteration scheme converges poorly outside the range given in figure 3, when the formulation using  $g(r, \phi)$  in (3.6) should be preferred, as in the next section. Given the form of (3.6), we anticipate that  $k \propto \varepsilon$  for large  $\varepsilon$ . The limiting toroidal cross-section has  $z \in [0, 1/\varepsilon]$ , which shrinks as  $\varepsilon$  grows. When  $n = 1$  in (3.1),  $k$  increases with  $z_0$ . However, when  $n = 0$ ,  $k$  is independent of  $z_0$ , with the smallest value given by taking  $\kappa = k/\varepsilon$  in (3.2). In the toroidal limit therefore this becomes the smallest overall and so we expect that  $k \sim 2.8596 \varepsilon$  as  $\varepsilon \rightarrow \infty$  in figure 3(a). The agreement seems to be good.

### 3.3.2. Circular helix

We now focus attention on a helical pipe with circular cross-section. This is the more interesting of the two cases from a physiological perspective. The coordinate system to be used is that of ZM. Most of the background details are given in the Appendix.

Taking the centreline of the circular pipe to be the helix with tangent vector  $\mathbf{H}_b = \mathbf{H}|_{r=b}$ , we fix local polar coordinates  $(\rho, \eta)$  with origin on the centreline in a

plane normal to  $\mathbf{H}_b$  so that the pipe surface is  $\rho = 1$ . Putting  $\hat{\mathbf{s}} = h_b \mathbf{H}_b$ ,  $x_3 = z$  in §2.1, we seek solutions to  $\nabla^2 V = 0$  in the form  $V = \text{Re}\{\exp(kz)f(\rho, \eta)\}$ . This leads to the following equation for  $f(\rho, \eta)$ :

$$f_{\rho\rho} + \frac{h^2}{r^2 J^2} f_{\eta\eta} + S f_\rho + T f_\eta - 2\epsilon k(\rho_\phi f_\rho + \eta_\phi f_\eta) + k^2 f = 0, \quad (3.9)$$

with boundary condition  $\mathbf{e}_\rho \cdot \nabla f = 0$  on the pipe surface. Thus

$$f_\rho - \epsilon k \rho_\phi f = 0 \quad \text{on} \quad \rho = 1. \quad (3.10)$$

The form of  $S$ ,  $T$  and the Jacobian  $J$  are given in the Appendix. Note that in the limit  $\epsilon \rightarrow 0$ ,  $h^2/(r^2 J^2) \rightarrow 1/\rho^2$ ,  $S \rightarrow 1/\rho$ ,  $T \rightarrow 0$ , and both  $\rho_\phi, \eta_\phi \sim O(1)$ , so the problem for the straight pipe is recovered.

Alternatively we may seek solutions in the form  $V = \text{Re}\{\exp(\kappa\theta)g(\rho, \eta)\}$ , where  $\kappa = k/\epsilon$ . This produces an equation and boundary condition which may be transformed to (3.9) with (3.10) by writing  $g = \exp(-\kappa\phi)f(\rho, \eta)$ . We will refer to these two equivalent formulations as  $kz$  and  $\kappa\theta$  respectively.

Unlike the rectangular helix considered previously, this pipe retains its circular cross-section for all values of  $\epsilon$ . Therefore, at  $\epsilon = 0$  we have a straight circular pipe with  $\mathbf{e}_z$  tangent to its centreline, and when  $\epsilon = \infty$  we have a circular torus with  $\mathbf{e}_t$  as its centreline tangent.

The numerical method of solution is the same as for the rectangle. Equation (3.9), along with the boundary condition (3.10) were approximated with centred differences, and the whole system was written as a matrix whose entries are at most quadratic in  $k$ . Periodicity in  $\eta$  was imposed in an obvious manner. The Lancaster iteration scheme was then employed at each value of  $\epsilon$  to converge to the required solution branch. Standard methods were used to deal with the coordinate singularity at  $\rho = 0$ .

The  $kz$  formulation becomes inaccurate as  $\epsilon b$  becomes large, when the  $\kappa\theta$  arrangement is more appropriate. The two formulations should give  $k = \kappa$  at  $\epsilon = 1$ . In figure 5(a) we plot the computed decay rates for varying  $\epsilon$  (fixed  $b = 1.5$ ). The numerical agreement between the two formulations (indicated by the curved dotted line) is tolerable.

Although the imaginary parts have not been plotted in figure 5(a), the eigenvalue becomes complex as soon as  $\epsilon$  is made non-zero. It was remarked in §3.1.2 that the first eigenvalue for the straight circular pipe is degenerate. Thus it appears as a repeated root when  $\epsilon = 0$ , which subsequently divides into a complex-conjugate pair as soon as the torsion is increased. A straight square pipe is also degenerate in the first eigenvalue and so we would expect the picture to be qualitatively similar. The  $(r, \phi)$  'rectangular' helix considered above does not immediately split into a conjugate pair as the straight pipe is not square at  $\epsilon = 0$ .

That the first eigenvalue should become complex immediately in the current circular case is confirmed by a perturbation analysis about  $\epsilon = 0$ . The local small- $\epsilon$  expansion for the first eigenvalue is  $k = 1.841 \pm i\epsilon + O(\epsilon^2)$ . Numerical computation yields  $k = 1.841 \pm 0.0099i$  at  $\epsilon = 0.01$ .

In the limit  $\epsilon \rightarrow \infty$ , corresponding to a circular torus, the governing equation becomes self-adjoint and so all the eigenvalues are real, and the conjugate roots coalesce. Thus, as for the straight pipe, we expect the first eigenvalue to be degenerate. This is far less clear for the torus than for the straight pipe where it is obvious from symmetry. That the first eigenvalue for the circular torus is degenerate was noted in §3.2.2.

The most accurate numerical results for both formulations of the problem came

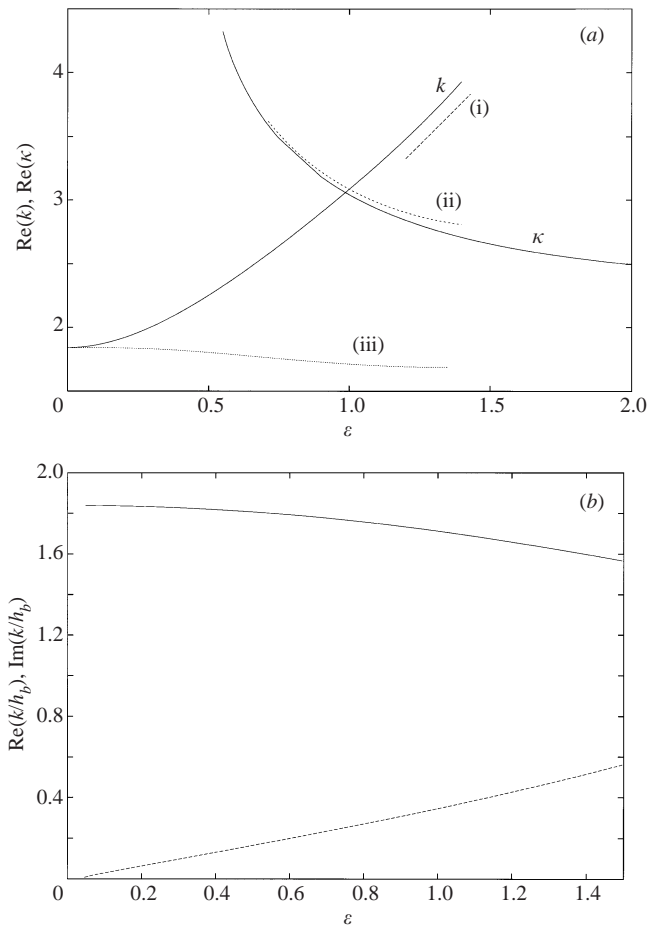


FIGURE 5. Numerical results for the circular helix of radius unity using a  $(30 \times 40)$  grid. Only the first eigenvalue is plotted. (a)  $b = 1.5$ :  $\text{Re}(k)$ ,  $\text{Re}(\kappa)$  (two solid lines) for the  $kz$ ,  $\kappa\theta$  formulations respectively, against  $\epsilon$ . The bottom line (iii) is  $\text{Re}(k)/h_b$  ( $h_b$  is the centreline arclength). The curved dotted line (ii) is  $k/\epsilon$  and should, in theory, agree with  $\kappa$ . The straight dotted line (i) is the expected limiting torus asymptote for  $k$ , of gradient 2.19 (which may be read off the curve in figure 2). (b)  $\text{Re}(k/h_b)$  (solid line) and  $\text{Im}(k/h_b)$  (dotted line) against  $\epsilon$  for  $\epsilon b = 1.5$  (fixed).

from where  $\epsilon b = O(1)$ . In order to show the effect of changing both  $b$  and  $\epsilon$  simultaneously therefore, in figure 5(b) we plot  $\text{Re}(k/h_b)$  and  $\text{Im}(k/h_b)$  against  $\epsilon$  with  $\epsilon b$  fixed. Note that the arclength along the helix centreline  $h_b$  remains constant in this instance, and that for physical reasons we must take  $b \geq 1$ . Once again  $\epsilon = 0$  corresponds to a straight pipe. This can be seen by allowing  $\epsilon \rightarrow 0$  in (3.9) and (3.10) with  $\epsilon b$  fixed, whereupon the equation for the straight pipe (with  $k$  replaced with  $k/h_b$ ) with boundary condition  $f_\rho(1) = 0$  is retrieved.

One final point on the numerical method employed here should be made. Although the circular torus is degenerate, and so the first eigenvalue should appear as a repeated root, we found that truncation errors caused it to bifurcate into a pair of roots whose real parts are close together. Thus as  $\epsilon$  is increased indefinitely in figure 5(a) the solid curve does not tend directly towards the desired asymptotic value but rather splits in two. We deem this to be an artifact of the discretization of the continuous system.

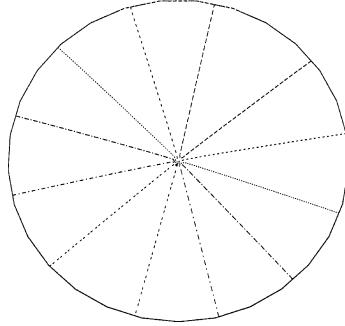


FIGURE 6. Contours of  $\psi - k_i z + \alpha$  at  $z = 0$  for the circular helix with  $\varepsilon = 0.1$ ,  $b = 1.5$ . The contours are equally spaced within the range  $[-\pi, \pi]$ .

This slight numerical ‘splitting’ of the eigenvalue also occurs in figure 5(b) at  $\varepsilon = 0$  and has been omitted from the graph.

#### 3.4. Interpreting complex decay rates

The implications for the flow when  $k$  is complex are not immediately obvious. For both the straight pipe and the torus, where  $k$  is real, we found that the downpipe velocity associated with the critical eigenfunction is zero on a surface with the same downpipe symmetry. The same is true for the helix as long as  $k$  is real. When  $k$  is complex, however, we find that such a surface still exists but it twists along the pipe.

For the helix the downpipe velocity is given by

$$u_H = h\mathbf{H} \cdot \nabla V = |kf| \operatorname{Re}\{e^{i(\psi - k_i z + \alpha)}\} e^{-k_r z} / h,$$

using the helical symmetry of  $f$ . Here we have written  $f = |f|e^{i\psi}$  and  $k = k_r + ik_i = |k|e^{i\alpha}$ . Thus  $u_H$  is zero when  $\psi - k_i z + \alpha = (2n + 1)\pi/2$ . Figure 6 shows contours of  $\psi - k_i z + \alpha$  at a fixed value of  $z$  for the circular helix. It is clear that a curve exists on which  $u_H$  is zero. Furthermore this curve will ‘rotate’ as  $z$  varies. There is no simple relation between this rotation rate and the helical pitch.

#### 3.5. Summary of the irrotational results

In this section we have calculated decay rates for the approach to inviscid, irrotational solutions in three distinct pipe geometries: a straight pipe, part of torus, and part of a helix. Our aim was to quantify the entry lengths required to attain fully developed potential solutions in these specific geometries, whilst providing generic results which might be used to interpret more complex flow development in non-uniform twists and bends. The following principal conclusions may now be stated regarding the evolution of potential flows from an arbitrary inlet velocity:

- (a) they are established most rapidly in a pipe which is perfectly straight;
- (b) the introduction of curvature or non-planarity serves to increase the entry length;
- (c) the eigenfunctions of the final mode to decay have a characteristic  $+/-$  structure, which is spatially dependent in the case of the helical pipe.

As detailed in §2.2, potential cores are to be expected for rapidly oscillating Womersley flows and for entry flows with an irrotational input. Even if the incoming fluid has vorticity, however, it may adjust to the symmetric pipe geometry on a lengthscale of order the pipe diameter, which can be determined in a similar manner to above. Such problems are discussed in the next section.

#### 4. Decay rates in rotational flows

In this section we aim to investigate how the presence of vorticity in the symmetric downstream state influences the rate at which it is approached. To this end we examine small perturbations to flow in a straight pipe and in part of a torus. The helical pipe will not be considered in this section. For the straight pipe, rotational profiles both with and without slip at the wall are considered. In the torus we take steady Dean-like flow as the background motion. Although in both geometries the effective Reynolds number is large, we assume implicitly that the basic flows are stable, and seek the mode with slowest spatial decay rate. We will sometimes encounter neutrally stable inertial waves, but these are less important for our purpose than the decaying modes. We are assuming that a flow is reached in a symmetric arterial portion which is almost independent of the downstream coordinate. In practice, this knowledge would come from MRI-imaging or some other scanning process. We then seek to estimate the length of artery, and in particular the upstream distance, over which this idealized flow can be expected to apply. The inertial wave perturbations do not grow in amplitude upstream but the decaying modes clearly will, and limit the upstream distance over which the observed solution is applicable. We thus obtain an estimate for the necessary inviscid entry length for the establishment of such a flow. It does not follow that such a flow will in fact occur if an artery exceeds this length, as an arbitrary input can give rise to nonlinear, large-amplitude inertial waves. Examples of inviscid non-decaying flows are discussed by Hawthorne (1955) and Sobey (1976). If the pipe section is too short, however, there is certainly no reason to expect an idealized solution to apply and the value of such approximations is questionable.

##### 4.1. Straight pipe

Steady fully developed viscous flow in a straight circular pipe adopts the Poiseuille profile. We consider a more general class of unidirectional Euler flows with the possibility of slip at the wall and calculate the rates of decay of exponentially small disturbances. The related problem of spatial stability of Poiseuille flow in a straight circular pipe was investigated by Gill (1965), and numerically by Garg & Rouleau (1972) for finite values of the Reynolds number and disturbance frequency.

We assume that the Reynolds number  $R$  is large and so viscous effects can be expected to be confined to the walls, and the inviscid core to vary slowly on an order-Reynolds-number downpipe lengthscale. We perturb this slowly developing base profile by admitting a small perturbation and writing

$$\mathbf{u} = u_0(r)\mathbf{e}_z + \exp(-kz)\mathbf{u}_1(r, \theta), \tag{4.1}$$

where the slow viscous evolution of the base flow  $u_0$  is neglected. We wish to solve for  $k$ ,  $\mathbf{u}_1$ , given  $u_0$ . The disturbance equations governing  $\mathbf{u}_1$ , obtained by substituting (4.1) into the Euler equations and linearizing, can be simplified to give a single relation for the perturbation pressure  $p_1(r, \theta)$ , namely

$$\nabla^2 p_1 - 2\frac{u_{0r}}{u_0}p_{1r} + k^2 p_1 = 0, \tag{4.2}$$

together with a wall condition to be discussed below and a regularity condition at the origin. Note that if the base flow is a constant then (4.2) reduces to the potential problem of §3.1 and hence in this case the smallest  $k$  is 1.841 for the first non-symmetric mode.

We consider two possibilities: either allowing  $u_0$  to have a slip velocity at the wall, or enforcing the viscous no-slip condition there. First we examine a base flow with

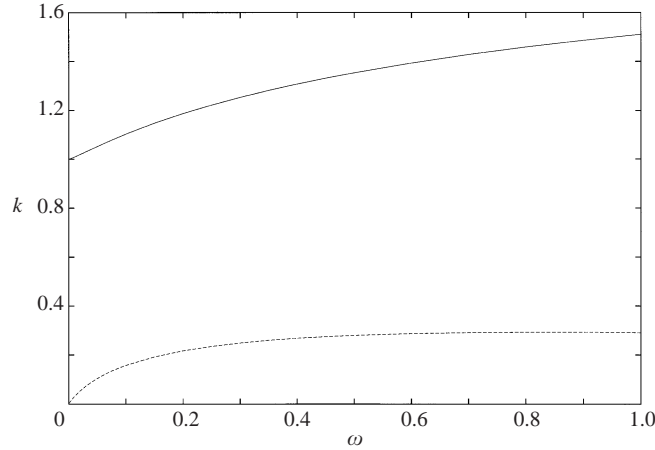


FIGURE 7.  $n = 1$ ,  $k = k_r + ik_i$ . Variation of  $k$  (solid line is  $k_r$ ; dashed line is  $k_i$ ) with  $\omega$ . Throughout the imposed boundary condition was  $p'_1(1) = 0$ . Note that in the limit  $\omega \rightarrow 0$ , this boundary condition changes abruptly to  $p(1) = 0$ .

no slip at the walls. We take the Poiseuille profile  $u_0 = 1 - r^2$ , even though in practice this would usually require an order-Reynolds-number entry length. The denominator in the second term of (4.2) has a zero at the wall, and the correct boundary condition is  $p(1) = 0$  (Smith 1976*b*). Then (4.2) admits the exact axisymmetric solution  $p = J_0(kr) + r^2 J_2(kr)$ , where  $J_i$  represents a Bessel function of the first kind. The smallest axisymmetric eigenvalue is the first zero of  $J_1(k) = 0$ , approximately 3.831, and this can be shown to be the smallest overall (Blyth & Mestel 1999).

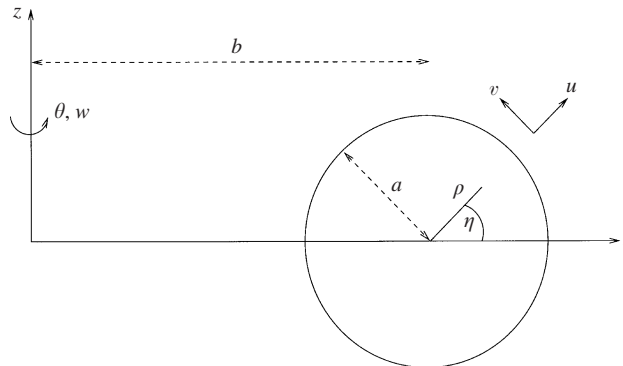
Now we permit slip at the wall and, by way of example, consider the base flow  $u_0 = 1 - \lambda r^2$ , for some constant  $\lambda$  between zero and one. There is no longer a zero in the denominator of the second term in (4.2), and in this case the correct wall condition is  $p'(1) = 0$ , which corresponds to tangential flow at the wall. The eigenvalues  $k$  must now be computed numerically. As  $\lambda \rightarrow 0$ , we recover the potential problem of § 3.1, for which  $k = 1.841$ . As  $\lambda \rightarrow 1^-$ , the no-slip case is approached, although we emphasize the change in the wall condition when  $\lambda = 1$ . We find that for  $\lambda < 1$  the eigenvalue is less than the value for the potential problem, and it approaches this value as  $\lambda \rightarrow 0$ . Thus with slip at the wall, as the vorticity in the base flow increases we find that the decay rate decreases from its irrotational value. In each case, the eigenfunction has a  $+/-$  structure. However, with no wall slip as above, the inviscid perturbations appeared paradoxically to decay much more quickly than either, and furthermore the eigenfunction was axisymmetric.

This paradox results from the zero of  $u_0$  at the wall when  $\lambda = 1$  and the resultant change in boundary condition. The singularity in the Rayleigh equation (4.2) can also be avoided by introducing a small time-dependence into the perturbation, writing

$$\mathbf{u} = u_0(r)\mathbf{e}_z + \text{Re}\{\exp(-kz - i\omega t + in\theta)\mathbf{u}_n(r)\},$$

for real non-zero  $\omega$  and integer  $n$ , where  $u_0 = (1 - r^2)$ . The denominator in the second term of (4.2) is then  $(u_0 - i\omega/k)$ , and the boundary condition  $p'(1) = 0$  applies once more. It is then found numerically that the first non-symmetric mode  $n = 1$  provides the eigenvalue  $k$  with the lowest real part. The variation of  $k$  with  $\omega$  for  $n = 1$  is shown in figure 7.

It can be seen from figure 7 that, as the disturbance frequency  $\omega$  approaches zero,


 FIGURE 8. Local polar coordinates  $(\rho, \eta)$  for the torus.

$\text{Re}(k) \rightarrow 1^+$  and  $\text{Im}(k) \rightarrow 0$  in agreement with Smith (1979). Smith stipulates that the slowest decaying modes are obtained when, in our notation,  $\omega \ll 1$  with  $|k| = O(1)$ . In this case the core plays a passive role, with the value of  $k$  determined by the viscous wall layer, and Smith demonstrates that  $k = n$ . The smallest decay rate is therefore  $k = 1$ .

We conclude that for profiles with no wall slip the decay is much slower when the disturbance has a small time-dependence, and the steady, inviscid results are misleading. For flows with wall slip, however, the inviscid analysis should apply.

#### 4.2. Curved pipes

In this section we will examine the decay rate of disturbances to rotational inviscid flows in curved pipes. The results may also apply to Euler flows with slow downstream development, e.g. Sobey (1976). As discussed above, we adopt high-Dean-number flow as the base state. For a circular cross-section we make the Dean approximation of small curvature, while the curvature is arbitrary for a rectangular pipe.

The background flow for the circular pipe has been the subject of much discussion. Experimental results (for example, those by Agrawal *et al.* 1978) have agreed well with numerical computations, notably those by Collins & Dennis (1975). Attempts have also been made, most recently by Dennis & Riley (1991), to describe the asymptotic structure in the high-Dean-number limit. These have not been completely successful however, owing to difficulties encountered at the inner wall. Even so, the favourable agreement between experiment and numerical computation is encouraging, and we anticipate that our results would be relevant to flows at large, but finite, Dean numbers.

We fix coordinates as shown in figure 8, with  $\theta$  measuring the angle about the  $z$ -axis, and with local polars  $\rho$  and  $\eta$  denoting radial distance within the cross-section and the local polar angle respectively. The pipe curvature parameter is defined to be  $\delta = a/b$ , where  $a$  is the radius of the cross-section, and  $b$  the radius of the pipe centreline.

All lengths are referred to the pipe radius  $a$ . The fluid velocity is written as  $(u, w, v) = \nu a^{-1}(u^*, \delta^{-1/2}w^*, v^*)$ , in  $(\rho, \theta, \eta)$ , where  $\nu$  is the kinematic viscosity of the fluid. Arclength  $s^*$  along the centreline satisfies  $as^* = b\theta$ . Asterisks are used here to denote dimensionless variables. In order that  $s^*$  derivatives should be retained in the equations we scale arclength as  $s^* = \delta^{-1/2}s$ , where  $s$  is of order unity. A pressure gradient  $-G$  is imposed in the  $\theta$ -direction to drive the main flow. The pressure is

non-dimensionalized as  $p = \rho_d v^2 p^* / a^2$ , for constant fluid density  $\rho_d$ . All asterisks will henceforth be dropped to avoid cluttering.

The steady flow is governed by the incompressible Navier–Stokes equations, which in the current coordinate system take the form (when  $\delta$  is small)

$$uu_\rho + vu_\eta/\rho + wu_s - v^2/\rho - \cos \eta w^2 = -p_\rho + \text{viscous}, \quad (4.3a)$$

$$uw_\rho + vv_\eta/\rho + wv_s + uv/\rho + \sin \eta w^2 = -p_\eta/\rho + \text{viscous}, \quad (4.3b)$$

$$uw_\rho + vw_\eta/\rho + ww_s = D - \delta p_s + \text{viscous}, \quad (4.3c)$$

$$u_\rho + u/\rho + v_\eta/\rho + w_s = 0. \quad (4.3d)$$

Here the Dean number is defined as  $D = Ga^3 \delta^{1/2} / (\rho_d v^2)$ , assumed large. For  $D \ll 1$  the flow deviates slightly from Poiseuille (Dean 1927, 1928). Except inside the boundary layer at the pipe wall, the viscous terms are all small for  $D \gg 1$ , and since we intend to concentrate on the inviscid part of the flow, they have not been detailed here. They may be found in Stewartson *et al.* (1980) for example.

Let  $\varepsilon \ll D^{1/3}$ , where  $\varepsilon$  is now an arbitrary small parameter, and  $D$  is large but finite. Taking the large-Dean-number asymptotic structure proposed by Dennis & Riley (1991) as the basis for our perturbation, we admit disturbances to the flow in the form (for  $s > 0$ )

$$w = D^{2/3} W_0(\rho, \eta) + D^{1/3} W_1(\rho, \eta) + \cdots + \varepsilon \exp(ks) w_1(\rho, \eta) + \cdots, \quad (4.4a)$$

$$u = D^{1/3} U_0(\rho, \eta) + \cdots + \varepsilon \exp(ks) u_1(\rho, \eta) + \cdots, \quad (4.4b)$$

$$v = D^{1/3} V_0(\rho, \eta) + \cdots + \varepsilon \exp(ks) v_1(\rho, \eta) + \cdots, \quad (4.4c)$$

$$p = D^{4/3} P_0(\rho, \eta) + \cdots + D^{2/3} \delta^{-1} \varepsilon \exp(ks) p_1(\rho, \eta) + \cdots, \quad (4.4d)$$

where the eigenvalue  $k$  is to be determined. In general it will be complex. The fully developed background flow  $\mathbf{U} = D^{2/3}(0, W_0, 0) + D^{1/3}(U_0, W_1, V_0) + \cdots$  is that computed numerically, for large finite  $D$ , by Collins & Dennis (1975) and other authors. It takes the general form  $W_0(\rho \cos \eta) = W_0(r - b)$ , and  $\psi = \rho \sin \eta / W_0'(\rho \cos \eta)$  where  $U_0 = \rho^{-1} \partial \psi / \partial \eta$ ,  $V_0 = -\partial \psi / \partial \rho$ . The exact form of  $W_0$  is decided by the solution of the boundary layer at the wall. Collins & Dennis found it numerically (see their figure 7), and their calculations agree very favourably with the experimental results of Agrawal *et al.* (1978). It is approximately linear in the core, increasing monotonically with  $r$ .

The perturbed equations in the core are

$$ku_1 - 2 \cos \eta w_1 = -p_{1\rho} / W_0, \quad (4.5a)$$

$$kv_1 + 2 \sin \eta w_1 = -p_{1\eta} / (\rho W_0), \quad (4.5b)$$

$$u_1 W_{0\rho} + v_1 W_{0\eta} / \rho + k W_0 w_1 = -k p_1, \quad (4.5c)$$

$$u_{1\rho} + u_1 / \rho + v_{1\eta} / \rho + k w_1 = 0. \quad (4.5d)$$

Note that if we change the sign of  $k$ , a sign change in  $w_1$  and  $p_1$  leaves these equations unaltered. So the eigenvalue can take either sign in what follows, with the appropriate sign changes in the eigenfunctions. Equations (4.5) also apply to perturbations of a general slowly developing inviscid flow  $W_0(r; s, t)$ .

We believe that the correct boundary condition is that of no flow into the boundary layer, namely

$$u_1(1, \eta) = 0. \quad (4.6)$$



Otherwise, if  $u_1(1, \eta) \neq 0$ , mass continuity in the boundary layer would require  $w_1$  to be singular at the wall, an eventuality which (4.5) does not permit since, unlike for Poiseuille flow,  $W_0$  is non-zero on the wall. Note that the background flow itself does allow a non-vanishing radial velocity at the wall since the downpipe component is an order of magnitude larger, and thus no imbalance in mass transport is encountered.

The velocities may be eliminated from the perturbation system (4.5) to reduce them to a single relation for the pressure  $p_1$  (compare equation (4.2)). However, the equation for  $p_1$  so produced, with its concomitant boundary condition, is somewhat unwieldy and instead we preferred to keep the equations in the given form. The individual components were analysed spectrally in  $\eta$ , with finite differences employed in  $\rho$ . Thus

$$(w_1, u_1, v_1, p_1) = \sum_{m=-M}^M (\hat{w}_m, \hat{u}_m, -i\hat{v}_m, \hat{p}_m) e^{im\eta},$$

where, due to symmetry,  $\hat{w}_m = \hat{w}_{-m}$ ,  $\hat{u}_m = \hat{u}_{-m}$ ,  $\hat{v}_m = -\hat{v}_{-m}$ , and  $\hat{p}_m = \hat{p}_{-m}$  for  $m = 1, \dots, M$ . A similar decomposition is used for the background flow  $W(\rho \cos \eta)$ . The sine and cosine terms in (4.5a) and (4.5b) provoke interaction between the modes, and so each eigenvalue  $k$  is determined by the whole truncated spectrum. Equations (4.5) are rearranged into the matrix form  $\mathbf{A}\mathbf{u} = k\mathbf{u}$ , where  $\mathbf{u}$  is the vector of velocity components for each mode at every grid point. This sparse system is then solved for the eigenvalues  $k$  using the Nag routine F02BCF.

Since the function  $W_0$  is more or less linear in  $\rho$ , rather than recompute the background flow we approximated it as

$$W_0 = 1 + B\rho \cos \eta,$$

where  $B$  is a constant. Only one free constant is required since (4.5) are invariant under the transformation  $(W_0, p_1) \mapsto c(W_0, p_1)$  for constant  $c$ .

The resulting smallest positive eigenvalues  $k$  are plotted against  $B$  in figure 9. When  $B = 1$ ,  $W_0$  develops a zero at  $\rho = 1$  when  $\eta = \pi$ , and the nature of the boundary condition (4.6) is called into question since now the possibility of singular behaviour of  $u_1$  arises at the wall. However, this is of secondary interest since, from Collins & Dennis' graph, we estimate  $B \approx 0.72$ . For this the smallest positive eigenvalue is  $k = 2.02$ . The corresponding eigenfunctions are plotted in figure 10. It shows contours of downpipe perturbation  $w_1$  and pressure perturbation  $p_1$  in the cross-section, and also a velocity vector plot of the cross-sectional flow  $(u_1, v_1)$ .

#### 4.2.1. Inertial waves

For any  $0 < B < 1$  there appear to exist infinitely many standing inertial waves corresponding to discrete values of  $k^2 < 0$ . For  $B = 0$  only positive values of  $k^2$  are found. If, using our estimate from Collins & Dennis, we take  $B = 0.72$ , we find, for example,  $k = 1.38i$ . Figure 11 shows contours of  $w_1$ ,  $p_1$  and a vector plot of the cross-sectional flow for this value. Further evidence for the existence of these waves was obtained by considering perturbations to Dean flow in part of a rectangular torus (see §4.2.2). We can show that they are consistent with the viscous wall layer described in Dennis & Riley (1991), at least near the outer bend. The asymptotic behaviour as  $D \rightarrow \infty$  near the inner bend is still not fully resolved, even for the base flow.

#### 4.2.2. Varying the curvature for a rectangular torus

So far we have kept the pipe curvature fixed (and small). We now investigate decay rates in pipes of differing uniform curvature. We will keep the geometry simple by

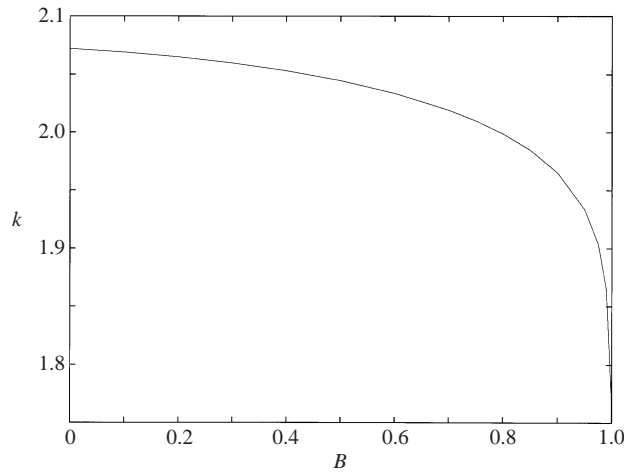


FIGURE 9. Smallest positive eigenvalues  $k$  versus background flow parameter  $B$ .

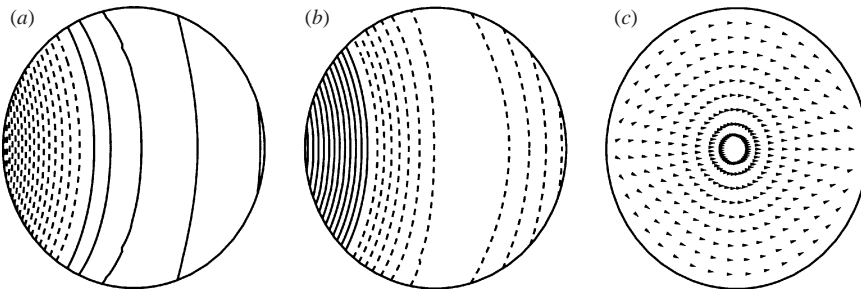


FIGURE 10.  $B = 0.72$ ,  $k = 2.02$ : Contours of (a) downpipe perturbation  $w_1(\rho, \eta)$  and (b) pressure perturbation  $p_1(\rho, \eta)$  in the cross-section. (c) Vector plot of  $(u_1, v_1)$ , the flow in the cross-section. Solid/dotted lines indicate positive/negative contours.

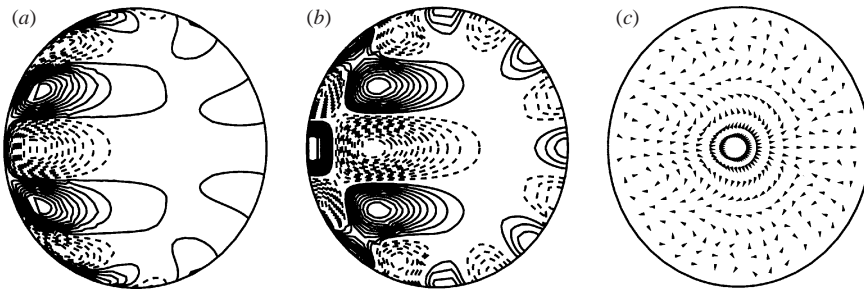


FIGURE 11. Inertial wave with  $k = 1.38i$ .  $B = 0.72$ : contours of (a) downpipe perturbation  $w_1(\rho, \eta)$  and (b) pressure perturbation  $p_1(\rho, \eta)$  in the cross-section. (c) Vector plot of  $(u_1, v_1)$ , the flow in the cross-section. Solid/dotted lines indicate positive/negative contours.

considering the perturbed flow in a rectangular torus. The background flow has been studied in detail by Smith (1976a). We will assume that the boundary layers remain attached to the walls.

The cross-section is defined to be  $z = 0, z_0$ , and  $r = b \pm a$ , with  $(u, w, v)$  denoting speeds in the  $(r, \theta, z)$  directions respectively. We permit only steady perturbations to the main flow. Following (4.4) we write  $w = D^{2/3}W_0(r) + \dots + \varepsilon \exp(k\theta)\tilde{w}$ , and so on,

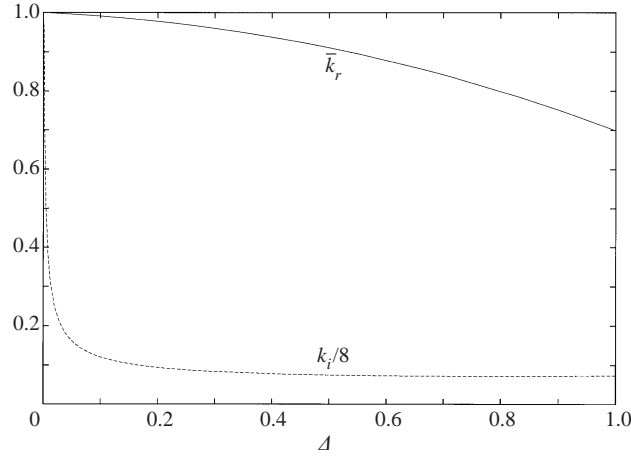


FIGURE 12. (a) Plot of smallest real  $k$  (plotted as  $\bar{k}_r = k_r/b$ ) and largest imaginary  $k$  (plotted as  $k_i/8$  for convenience) against rectangular curvature  $\Delta$  when  $m = 1$  for fixed  $2a = 1$ ,  $z_0 = \pi$ ,  $\gamma = 0.5$ .

to produce the following set of disturbance equations in the inviscid core:

$$kW_0u_1/r - 2W_0w_1/r = -p_{1r}, \quad (4.7a)$$

$$kW_0w_1/r + W_0u_1/r + W_{0r}u_1 = -kp_1/r, \quad (4.7b)$$

$$kW_0v_1/r = m\pi p_1/z_0, \quad (4.7c)$$

$$u_{1r} + u_1/r + kw_1/r + m\pi v_1/z_0 = 0, \quad (4.7d)$$

where we have taken  $(\tilde{u}, \tilde{w}, \tilde{p}) = (u_1, w_1, p_1) \cos(m\pi z/z_0)$ , and  $\tilde{v} = v_1 \sin(m\pi z/z_0)$  for integer  $m$  to satisfy the solid boundary condition at  $z = 0, z_0$ . The background flow function is taken to be of the form  $W_0 = 1 + \gamma(r - b + a)$  for constant  $\gamma$ . We calculate eigenvalues  $k$  for different uniform curvatures  $\Delta = 2a/b$ . Since higher modes provide qualitatively similar results, we will take  $m = 1$ .

We fix  $2a = 1$ ,  $z_0 = \pi$  and  $\gamma = 0.5$ . The curvature  $\Delta$  is then allowed to vary. For any fixed  $\Delta$  we find both real ( $\pm k_r$ ) and imaginary ( $\pm ik_i$ ) eigenvalues, but none which are complex. There are finitely many imaginary eigenvalues. The smallest  $k_r$  and the largest  $k_i$  are plotted in figure 12. The largest  $k_i$  increases indefinitely as  $\Delta$  approaches zero. This lends some credence to the suggestion in §4.2.1, for the circular torus, that in the Dean limit of zero curvature there is an infinite number of imaginary eigenvalues. We are primarily interested in the perturbation decay rates, which correspond to the real eigenvalues divided by the radius of the centreline. We write  $\bar{k}_r = k_r/b$ . As the curvature tends to zero, with  $a$  fixed, we find that  $\bar{k}_r$  approaches unity from below. This can readily be seen by taking the appropriate limit in the equations. These results broadly support those found for the circular torus in the limit of zero curvature ( $\delta = 0$ ). Furthermore  $\bar{k}_r$  steadily decreases with increasing  $\Delta$ , suggesting that a more rapid decay rate would also be found for the circular torus if  $\delta$  were positive.

In reality we know that  $\gamma > 0$  for the background flow. However, if we allow  $\gamma < 0$  we find that, as  $\Delta \rightarrow 0$  with  $a$  fixed, all of the eigenvalues  $k^2$  eventually become positive, and in the limit it seems that no inertial waves exist for the rectangular case. This remark is supported by a calculation for the circular torus (at zero curvature)

with  $B = -0.72$ . In this case it is also found that all  $k^2 > 0$  and so no inertial waves are present.

#### 4.3. *Summary of the rotational results*

In this section we have investigated how the introduction of vorticity affects the decay rates in pipe flows. We looked at perturbations to unidirectional flows in a straight pipe at high Reynolds number and to flow in a curved pipe at high Dean number. In both cases the background flows are composed of an inviscid rotational core with an attached boundary layer at the wall. Helical pipes were not considered. Our conclusions are as follows.

For the straight pipe at high Reynolds number:

(a) in the absence of wall slip, unsteady disturbances of very small frequency decay the slowest;

(b) with wall slip, steady perturbations decay more slowly the greater the vorticity.

For the curved pipe at high Dean number:

(a) increasing the curvature decreases the decay rate;

(b) for arbitrary curvature inertial waves can exist, presumably decaying on a much longer viscous lengthscale. However, as these waves do not grow in amplitude either up- or downstream, they do not affect the region of validity of the idealized flow which is being perturbed.

### 5. Overall summary and discussion

Given arbitrary steady inlet conditions, flow in pipes with suitable geometries requires certain entry lengths before a developed inviscid state can be reached, although as we have seen, this need not occur for rotational flows. Our aim here has been to quantify these distances by analysing the rate at which disturbances die out before the geometrically symmetric state is attained. We have calculated such decay rates for potential flow in a straight pipe, part of a torus of general uniform curvature, and a helical pipe of arbitrary curvature and pitch. In the limits of zero and infinite pitch the latter corresponds to a straight and toroidal pipe respectively. We have also computed decay rates for rotational flow in a straight pipe at large Reynolds number, and for a curved pipe at large Dean number. The potential results are applicable to Womersley-type flows, when the driving pressure gradient is fluctuating rapidly in time. They can also be applied to developing flows, assuming that the inlet profile is irrotational. For example our results might be used to model flow in the ascending aorta, at least during part of the cardiac cycle, if the blood is ejected from the heart without significant vorticity. The rotational decay rates are also informative since fully developed profiles are often used as entry conditions in CFD simulations with realistic arterial geometries when they may in fact be inappropriate. Truly viscous perturbations to otherwise fully developed profiles require long distances in which to decay. This is due to the slow growth of the boundary layers, which typically evolve on a lengthscale of the order of the Reynolds number. Inviscid, irrotational disturbances such as those studied in §3 decay much more rapidly down-stream, usually within a few pipe diameters. The same is true for the decaying modes in rotational flows considered in §4, although waves may also exist in that case. An important viscous effect is the possible separation of wall layers, which can occur on an  $O(1)$  lengthscale. However, as illustrated below, this often takes place much beyond the inviscid flow establishment.

We now summarize the general conclusions of this paper. The decay rates we have

Radius of curvature $b$	1.0	1.5	2.0	2.5	$\infty$
Potential	0.936	0.973	0.985	0.991	1
Rotational	0.700	0.855	0.911	0.938	1

TABLE 1. Lowest decay rate  $\kappa/b$  in the rectangular torus  $r = b \pm 0.5$ ,  $z = 0, \pi$ , for various  $b$ .

calculated were inviscid, even when fully developed viscous profiles were considered. The potential flow results indicate that in most cases the first non-symmetric mode is the most persistent. The corresponding eigenfunctions have a characteristic  $+/-$  structure, with a dividing line on which the downpipe velocity is zero. Disturbances decay fastest in a perfectly straight pipe and slowest in a torus, with those in a helical pipe somewhere in between.

For steady disturbances to Poiseuille flow in a straight circular pipe, the axisymmetric mode is the most resilient. However, in this case slightly unsteady non-symmetric modes can decay more slowly, in line with the results of Smith (1979). If these modes are taken into account, the core flows with slip are established more quickly than those without.

For the curved pipe at high Dean number, the notion of an inviscid decay rate was clouded somewhat by the presence of standing inertial waves of fixed amplitude. A finite number of these waves exist for non-zero curvature, but in the Dean limit of zero curvature there are apparently infinitely many. If present, these waves are presumably eventually damped out by viscosity. Alternatively, they could be excluded mathematically by a suitable downstream condition, but as they do not influence our conclusions greatly, and reflect a genuine physical tendency of Euler flows, we have included them. They should not be confused with the large-amplitude nonlinear structures which may evolve from an arbitrary inlet.

Table 1 compares the  $\theta$  decay rate per unit arclength  $\kappa/b$  of the final streamwise mode in a rectangular torus of dimension  $r = b \pm 0.5$ ,  $z = 0, \pi$  for the potential and rotational (high Dean number) cases. The potential decay rates were calculated using (3.1). The rotational ones may be read off the graph in figure 12. In each case disturbances decay more slowly in a torus than a straight pipe. This can be seen as a direct result of the curvature, suggesting that disturbances to flows leaving a bend and entering a straight section are likely to persist for a shorter distance than those coming into a curved pipe. As  $b$  increases the potential decay rate approaches the straight pipe limit (§3.1.1), while the rotational ones tend to the Dean limit of zero curvature (§4.2.2). In both cases this limit is unity. The effect of torsion, for fixed curvature, on irrotational decay rates in a circular pipe is seen from line (iii) in figure 5. The decay rate per unit arclength  $k/h_b$  decreases monotonically from its value in a straight pipe ( $\varepsilon = 0$ ) to that in a torus ( $\varepsilon \rightarrow \infty$ ). Thus, increasing the torsion means perturbations decay more slowly. We have not assessed the effects of non-planarity for rotational disturbances, although similar conclusions are to be expected.

Finally, we summarize the implications of this work for physiologists. First, if circumstances are such that the flow can be considered rapidly oscillating or potential, we have quantified the distance over which an arbitrary inlet flow will evolve to the developed state. If however the flow has a rotational core, while we have calculated the necessary inviscid entry length, it cannot be guaranteed that an arbitrary initial flow will adjust to a state with the appropriate geometrical symmetry because of inertial oscillations. Yet if observations do indicate that an appropriate Euler flow is

nearly attained at some point in the artery, then we have found the extent of validity of this flow. Curiously, a smaller decay rate would then indicate a larger region of ideal flow.

If a symmetric state is indeed established, the rotational and irrotational results are qualitatively similar. The introduction of curvature (and for the potential case non-planarity) into the pipe geometry tends to lower the rate at which disturbances to the background flow decay. Thus the introduction of vorticity does not alter the general effects of changes in curvature. The persistence of flow perturbations when curvature is non-zero might be regarded as beneficial from a physiological standpoint, since prolonged swirl will promote more efficient cleaning of the arteries.

Using this work, we can identify regions of the arterial tree in which idealized flow models might be applicable. For example, the human aortic arch has a typical diameter of 1.25 cm and curvature radius 3.125 cm, and the inflow from the heart is more or less irrotational during systole. The distance to boundary layer separation at the inner wall is 5.56 cm (Riley 1998), while our calculations show that input disturbances halve in magnitude every 0.63 cm. There is thus sufficient distance for the flow to develop. However, our results also show that at other places in the arterial tree there is unfortunately little *a priori* justification for assuming idealized flow, contrary to popular practice. Analytical or numerical simulations with idealized inflow should thus be treated with caution.

We gratefully acknowledge the support of The Wellcome Trust in performing this work.

## Appendix

In this Appendix we fill in a few of the missing details from the beginning of §3.3.2. The remainder can be found in Zabielski & Mestel (1998*a*, referred to herein as ZM). The pipe centreline is the helix with tangent vector  $\mathbf{H}_b = \mathbf{H}|_{r=b}$ . Local polar coordinates  $(\rho, \eta)$  are fixed with origin on the centreline in a plane normal to  $\mathbf{H}_b$  so that the pipe surface is  $\rho = 1$ . It can then be shown that

$$r^2 = (b + \rho \cos \eta)^2 + \rho^2 \sin^2 \eta / h_b^2, \quad (\text{A } 1)$$

$$\phi = \tan^{-1} \left\{ \frac{\rho \sin \eta}{h_b(b + \rho \cos \eta)} \right\} + \varepsilon^2 b \rho \sin \eta / h_b. \quad (\text{A } 2)$$

Recall that  $h(r) = (1 + \varepsilon^2 r^2)^{1/2}$ , and  $h_b = h(b)$ . As in ZM we construct the orthogonal vector base  $(\mathbf{e}_\rho, \mathbf{e}_\eta, \mathbf{H})$  wherein we make the definition  $\mathbf{e}_\rho = \nabla \rho$ , which leads to  $\mathbf{e}_\eta = h\mathbf{H} \times \mathbf{e}_\rho$ .

For non-helically symmetric functions it may be shown that

$$\nabla = \mathbf{e}_\rho(\partial_\rho + \varepsilon \rho_\phi \partial_z) + \mathbf{e}_\eta \left( \frac{h}{rJ} \partial_\eta + \frac{\varepsilon r}{h} \rho_r \partial_z \right) + \mathbf{H} \partial_z, \quad (\text{A } 3)$$

where  $\partial_z$  represents  $\partial/\partial z$  for example. The Jacobian  $J = |\partial(r, \phi)/\partial(\rho, \eta)|$ , given explicitly in ZM. The coefficients  $S$  and  $T$  in (3.9) are defined as

$$S = \rho_{rr} + h^2 \rho_{\phi\phi} / r^2 + \rho_r / r,$$

$$T = \eta_{rr} + h^2 \eta_{\phi\phi} / r^2 + \eta_r / r.$$

The forms of  $\rho_r, \eta_r$  etc. may be obtained from ZM, although we here note a misprint

in their given form of  $\eta_{\phi\phi}$ . The final term should read

$$-\frac{\partial J/\partial\phi}{2rJ^2}(2\cos\eta(b+\rho\cos\eta)+2\rho\sin^2\eta/h_b^2).$$

## REFERENCES

- AGRAWAL, Y., TALBOT, L. & GONG, K. 1978 Laser anemometer study of flow development in curved circular pipes. *J. Fluid Mech.* **85**, 497–518.
- BERGER, S. A., TALBOT, L. & YAO, L. S. 1983 Flow in curved pipes. *Annu. Rev. Fluid Mech.* **15**, 461–512.
- BLYTH, M. G. & MESTEL, A. J. 1999 Steady flow in a dividing pipe. *J. Fluid Mech.* **401**, 339–364.
- CHANDRAN, K. B. 1993 Flow dynamics in the human aorta. *J. Biomech. Engng* **115**, 611–616.
- COLLINS, W. M. & DENNIS, S. C. R. 1975 The steady motion of a viscous fluid in a curved tube. *Q. J. Mech. Appl. Maths* **28**, 133–156.
- DEAN, W. R. 1927 Note on the motion of fluid in a curved pipe. *Phil. Mag.* **4**, 208–223.
- DEAN, W. R. 1928 The streamline motion of a fluid in a curved pipe. *Phil. Mag.* **5**, 673–695.
- DENNIS, S. C. R. & RILEY, N. 1991 On the fully developed flow in a curved pipe at large Dean number. *Proc. R. Soc. Lond. A* **434**, 473–478.
- DRAZIN, P. G. 1977 On the stability of cnoidal waves. *Q. J. Mech. Appl. Maths* **30**, 91–105.
- GARG, V. K. & ROULEAU, W. T. 1972 Linear spatial stability of pipe Poiseuille flow. *J. Fluid Mech.* **54**, 113–127.
- GILL, A. E. 1965 On the behaviour of small disturbances to Poiseuille flow in a circular pipe. *J. Fluid Mech.* **21**, 145–172.
- HAWTHORNE, W. R. 1955 The growth of secondary circulation in frictionless flow. *Proc. Camb. Phil. Soc.* **51**, 737–743.
- HUERRE, P. & MONKEWITZ, P. A. 1990 Local and global instabilities in spatially developing flows. *Annu. Rev. Fluid Mech.* **22**, 473–537.
- KU, D. N. 1997 Blood flow in arteries. *Annu. Rev. Fluid Mech.* **29**, 399–434.
- LAM, S. T. 1988 On high Reynolds number laminar flows through a curved pipe, and past a rotating cylinder. PhD thesis, Imperial College, London.
- LANCASTER, P. 1966 *Lambda-Matrices and Vibrating Systems*. Pergamon.
- LYNCH, D. G., WATERS, S. L. & PEDLEY, T. J. 1996 Flow in a tube with non-uniform, time-dependent curvature: governing equations and simple examples. *J. Fluid Mech.* **323**, 237–265.
- MCDONALD, D. A. 1974 *Blood Flow in Arteries*. Southampton: The Camelot Press Ltd.
- MORSE, P. M. & FESHBACH, H. 1953 *Methods of Theoretical Physics*. McGraw-Hill.
- PEDLEY, T. J. 1980 *The Fluid Mechanics of Large Blood Vessels*. Cambridge University Press.
- PEDLEY, T. J. & STEPHANOFF, K. D. 1985 Flow along a channel with a time-dependent indentation in one wall – the generation of vorticity waves. *J. Fluid Mech.* **160**, 337–367.
- RILEY, N. 1998 Unsteady fully-developed flow in a curved pipe. *J. Engng Maths* **34**, 131–141.
- SINGH, M. P. 1974 Entry flow in a curved pipe. *J. Fluid Mech.* **65**, 517–539.
- SMITH, F. T. 1976a Steady motion within a curved pipe. *Proc. R. Soc. Lond. A* **347**, 345–370.
- SMITH, F. T. 1976b Flow through constricted or dilated pipes and channels: Part 2. *Q. J. Mech. Appl. Maths* **29**, 365–376.
- SMITH, F. T. 1979 Instability of flow through pipes of general cross-section. *Mathematika* **26**, 187–210.
- SMITH, F. T. & BODONYI, R. J. 1982 Amplitude-dependent neutral modes in the Hagen–Poiseuille flow through a circular pipe. *Proc. R. Soc. Lond. A* **384**, 463–489.
- SOBEY, I. J. 1976 Inviscid secondary motions in a tube of slowly-varying ellipticity. *J. Fluid Mech.* **73**, 621–639.
- STEWARTSON, K., CEBECI, T. & CHANG, K. C. 1980 A boundary layer collision in a curved duct. *Q. J. Mech. Appl. Maths* **33**, 59–75.
- STEWARTSON, K. & STUART, J. T. 1971 A nonlinear instability theory for a wave system in plane Poiseuille flow. *J. Fluid Mech.* **48**, 529–545.
- YAO, L.-S. & BERGER, S. A. 1975 Entry flow in a curved pipe. *J. Fluid Mech.* **67**, 177–196.
- ZABIELSKI, L. & MESTEL, A. J. 1998a Steady flow in a helically symmetric pipe. *J. Fluid Mech.* **370**, 297–320 (referred to herein as ZM).
- ZABIELSKI, L. & MESTEL, A. J. 1998b Unsteady blood flow in a helically symmetric pipe. *J. Fluid Mech.* **370**, 321–345.